EFFICIENT NUMERICAL PROPAGATION OF PLANETARY CLOSE ENCOUNTERS WITH REGULARIZED ELEMENT METHODS

Davide Amato, Claudio Bombardelli

Technical University of Madrid
School of Aerospace Engineering
Space Dynamics Group
Plaza Cardenal Cisneros, 3
28040 Madrid (ES)

Giulio Baù

University of Pisa
Department of Mathematics
Largo Bruno Pontecorvo, 5
56127 Pisa (IT)

ABSTRACT

Close encounters with major Solar System bodies may bring about a strong amplification of numerical error during interplanetary orbit propagation. In this work, we reduce global numerical error by integrating regularized equations of motion instead of the classical Newtonian equations in Cartesian coordinates. The integration performance of several sets of regularized equations is assessed from large-scale numerical propagations of close encounters in the Sun-Earth planar CR3BP. An essential device consists in switching between primary bodies during the propagation, which effectively decomposes a strongly-perturbed heliocentric problem into two weakly-perturbed ones; this propagation approach has been dubbed *Online Trajectory Matching* (OTM). Through this simple expedient, regularized equations describing the evolution of non-classical orbital elements achieve excellent performances compared to Newtonian equations, even when employing sophisticated adaptive numerical schemes. Further improvements might be expected by carefully selecting the location of the switch of primary bodies during the propagation.

Index Terms— Close encounters, regularization, numerical methods, special perturbations

1. INTRODUCTION

Accurately predicting the outcome of planetary close encounters is a momentous task in dynamical astronomy, which finds critical applications in Space Situational Awareness and spacecraft mission design.

Planetary close encounters are the only natural phenomenon capable of modifying the orbit of a Solar System object on a short heliocentric time scale. Their importance in shaping the dynamics of the Solar System has resulted in them being extensively studied in dynamical astronomy, and several analytical techniques have been developed to predict their outcome in terms of heliocentric orbital elements.

For instance, Öpik [1] developed a seminal technique which is often used in statistical studies of asteroid and cometary close encounters, and it has been used to discover by purely dynamical means the existence of a period of Late Heavy Bombardment in the history of the Inner Solar System. His work was later expanded by Valsecchi et al. to non-zero minimum approach distances and small inclinations [2, 3]. This theory is now widespread for the prediction of encounter outcomes by Near-Earth Asteroids (NEAs) and possible resonant returns.

However, analytical theories do not allow to reach very high accuracies due to the approximations involved. If high accuracies are required, it is necessary to resort to special perturbation techniques. Even in this case some care is needed in numerical propagations, since a close encounter will inevitably compromise the quality of a solution if not properly taken into account. A widely adopted technique is to employ an adaptive numerical scheme, that is one which is capable of modifying its step size and/or its order as to minimize the local truncation error on the basis of some criterion, e.g. the instantaneous estimation of the eigenvalues of the Jacobian of the equations of motion [4].

Another common approach used to increase the numerical efficiency, which stems from the field of dynamical astronomy, is to integrate *regularized* equations of motion, i.e. equations from which the singularity for $r = 0$ has been eliminated through analytical means [5]. If the problem is weakly perturbed, further advantages can be obtained by integrating equations of motion relative to orbital elements, which evolve quite smoothly under the action of small perturbations. This last approach has already proven to improve the accuracy in the propagation of resonant close encounters [6].

In this work, we are concerned with improving the quality of numerical propagations of interplanetary close encounters by applying the aforementioned techniques. In particular, we will assess the efficiency of integrating close encounters with a family of two regularized element methods of the *Dromo* family [7, 8], which have shown excellent numerical perfor-

mances and whose main features are presented in Section 2 along with the main characteristics of regularized formulations of dynamics. The physical model used to reproduce close encounters is described in Section 3. Section 4 deals with the propagation strategy devised to increase the propagation efficiency of the Dromo element methods. The propagation error and computational cost metrics used for the study are described in Section 5. The performance analysis of the regularized formulations compared to the integration of the Newtonian equations (Cowell formulation) is carried out in Section 6. The conclusions of the study are summarized in Section 7.

2. REGULARIZATIONS AND ELEMENT METHODS

The Newtonian equations of motion in Cartesian coordinates in the presence of a perturbing acceleration $\boldsymbol{F}$,

$$\ddot{\boldsymbol{r}} = -\frac{\mu}{r^3}\boldsymbol{r} + \boldsymbol{F}, \tag{1}$$

present a singularity at collision ($r = 0$) which poses a burden for numerical integration. Even if the singularity is never actually reached, we can expect the solution to vary strongly when close to it. Therefore, it is difficult to approximate the solution by a numerical method in this situation, and accuracy (or computational time) will be inevitably affected. Also, every elliptic solution of (1) is unstable in the Lyapunov sense, which is unfavourable for the propagation of numerical error [9].

2.1. Regularization of the equations of motion

The issues connected to the presence of the singularity for $r = 0$ may be avoided by *regularizing* the equations of motion, that is eliminating the singularity for $r = 0$. This is achieved analytically in two steps. Firstly, the independent variable is changed from the *physical* to a *fictitious* time through a differential relation, the *Sundman transformation*. Secondly, one or more integrals of motion are embedded into the equations [10]. The resulting set of equations is often redundant, that is the number of first-order ODEs is greater than the number of degrees of freedom of the particle. Even with this penalization, regularization is still beneficial for numerical integration due to the elimination of the singularity and the analytical stabilization of the equations of motion [5].

One practical aspect regarding the implementation of regularized equations in an orbit propagation software deserves further attention. In most practical cases, the propagation has to be stopped at one or more values of the physical time t^*. However, in regularized formulations the physical time is a function of the fictitious time s, i.e. it is effectively one of the state vector variables. Therefore, the value s^* of the fictitious time which satisfies $t^* = t(s^*)$ must be found by an iterative process during or after the propagation [11]. This is an important requirement driving the choice of the numerical solver.

2.2. Element methods

One beneficial effect of regularization is to replace Equation (1) by linearized differential equations with coefficients which are constant in the unperturbed two-body problem. By applying the variation of parameters technique to these linearized equations it is possible to introduce first-integrals of the two-body problem. These new quantities, which are called orbital elements, can be used as state variables instead of the position and velocity. If the motion is weakly perturbed (which occurs commonly in astrodynamics) the solution expressed in terms of elements will deviate from the constant part on a slow time-scale. This enables a numerical integrator to take larger step sizes and therefore increase the propagation efficiency.

Not all element methods are suitable for any orbit type. In fact, some of them are particularized only for a given type of orbit, i.e. only for a given sign of the eccentricity or the total orbital energy.

Besides the classical (Keplerian) orbital elements, several other element sets have been developed, along with their equations of motion. A survey of element methods is available in Ref. [12].

2.3. Comparison of dynamical formulations

The formulations that we compared in the present work are summarized in Table 1, which gives the kind of state variables used (coordinates or elements), the type of orbit that can be described, and the number of ODEs to be solved in each formulation for a 3-dimensional problem.

The *Kustaanheimo-Stiefel* (K-S) regularization is one of the best known in dynamical astronomy; it is extensively described in the work by Stiefel and Scheifele [5].

In this formulation, the state of the particle is expressed through a 4-dimensional vector $\boldsymbol{u}$ which is the solution of a perturbed harmonic oscillator. The state vector is composed by ten quantities: the components of $\boldsymbol{u}$ and $\dot{\boldsymbol{u}}$, the total energy and the physical time.

EDromo and *HDromo* are two regularized element formulations which are closely related to a special perturbations method originally developed by Peláez et al. [13]. In this method, called *Dromo*, the orbital motion is described by the physical time and 7 spatial elements. These are the inverse of the angular momentum, two projections of the eccentricity vector along the axes of an ideal reference frame, and the components of a unit quaternion which describes the instantaneous orientation of this frame. *EDromo* and *HDromo* are restricted to negative and positive signs of the total orbital energy respectively. They also use a set of 7 orbital elements, three of which express the size and shape of the orbit and

Table 1: Formulations used in the work. "Cowell" refers to the numerical integration of the unregularized Newtonian equations, Equation (1). The quantity ε denotes the total energy, i.e. the sum of the Keplerian energy and the disturbing potential energy.

Formulation	Type	Orbit	ODEs
Cowell	Coord.	Any	6
Kustaanheimo-Stiefel	Coord.	Any	10
EDromo	Elem.	$\varepsilon < 0$	8
HDromo	Elem.	$\varepsilon > 0$	8

the remaining four constitute a quaternion, in analogy with Dromo. However, the adopted fictitious time is fundamentally different and a perturbing potential is introduced [7, 8].

3. PHYSICAL MODEL

As a benchmark model, we took the Sun-Earth planar, circular, restricted three-body problem (PCR3BP). The only perturbation is due to the gravitational attraction of the secondary body, so that the perturbing acceleration $\boldsymbol{F}$ in Equation (1) is expressed as

$$\boldsymbol{F} = -\mu' \left(\frac{\boldsymbol{d}}{d^3} + \frac{\boldsymbol{\rho}}{\rho^3} \right), \tag{2}$$

where μ' is the gravitational parameter of the secondary body and $\boldsymbol{d}$, $\boldsymbol{\rho}$ are the vectors from the primary body of attraction to the particle and to the perturbing body, respectively. The Sun and the Earth may switch roles as primary bodies during the propagation, according to the algorithm described in Section 4.1.

3.1. Close encounter parametrization

We assume that the close encounter takes place at time $t = 0$. Each propagation is parametrized by three quantities that completely define the close encounter. These are:

- d, the minimum approach distance;
- e, the eccentricity of the geocentric hyperbola at the minimum approach distance ($e > 1$);
- θ, the angle between the geocentric position vector at the minimum approach distance $\boldsymbol{d}$ and the Sun-Earth direction.

Two more parameters describing the hyperbolic encounter are of particular interest: the asymptotic velocity U and the asymptote angle φ. By the vis-viva and conic equations, we obtain U and φ from d and e as

$$U = \sqrt{\frac{\mu_\oplus}{d}\,(e-1)}, \tag{3}$$

$$\cos\varphi = \frac{1}{e}. \tag{4}$$

The encounter energy $\varepsilon > 0$ increases with U since $\varepsilon = U^2/2$. In this sense, we speak equivalently of *high-* (*low-*) energy and *fast* (*slow*) encounters. Note that increasing d results in decreasing the asymptotic velocity, but does not affect the asymptote angle. Increasing e increases both the asymptotic velocity and the asymptote angle φ, $0 < \varphi < \pi/2$. High encounter eccentricities correspond to hyperbolas which tend to be rectilinear, and to smaller deviation angles.

We consider a heliocentric reference system $\{O, x, y\}$ such that at $t = 0$ the Earth lies on the $x-$axis, at a distance of 1 au. The initial angle θ determines the orientation of the encounter in this frame. More specifically, varying θ changes the orientation of the incoming and outgoing geocentric asymptotic velocity vectors $\boldsymbol{U}^-, \boldsymbol{U}^+$ with respect to the Earth's heliocentric velocity vector $\boldsymbol{v}_\oplus$, as shown in Figure 1. The angle between $\boldsymbol{U}^-$ (equivalently, $\boldsymbol{U}^+$) and $\boldsymbol{v}_\oplus$ strongly affects the variation in the heliocentric orbital energy of the particle due to the close encounter.

Under the hypotheses of the matched-conics approximation [14], it is possible to derive analytically the pre- and post-encounter heliocentric orbital elements corresponding to given values of (d, e, θ). This allows us to write the pre- and post-encounter heliocentric orbital energies $\varepsilon^-, \varepsilon^+$ as a function of the close encounter parameters in a compact manner,

$$\varepsilon^{\mp} = \frac{U^2 - v_\oplus^2}{2} + U v_\oplus \sin(\varphi \pm \theta), \tag{5}$$

where the upper sign refers to the pre-encounter energy ε^-. It is important to highlight that while θ does not affect the type of geocentric trajectory, it does have an impact on the heliocentric orbital elements. In particular, both open and closed heliocentric orbits might correspond to a given pair (d, e), depending on the value of θ. Also, the variation in the heliocentric orbital energy can be written as

$$\Delta\varepsilon = \varepsilon^+ - \varepsilon^- = -2U v_\oplus \sin\theta \cos\varphi. \tag{6}$$

Therefore, $\Delta\varepsilon$ varies with $\sin\theta$. Values of $\theta = 0^\circ$ or 180° imply very similar pre- and post-encounter heliocentric orbits, which simplifies the analysis of the numerical experiments. The most violent close encounters (highest $\Delta\varepsilon$) are obtained with $\theta = 90^\circ, 270^\circ$.

4. PROPAGATION METHODOLOGY

We propagated interplanetary trajectories characterized by only one close encounter using two different approaches. In the first, the whole integration of the equations of motion is carried out in a heliocentric reference system, with the Sun as the primary body and the Earth as a perturber. In the second, the main gravitational body is switched from the Sun (Earth) to the Earth (Sun), when the geocentric distance of the propagated body becomes smaller (greater) than a given "switch

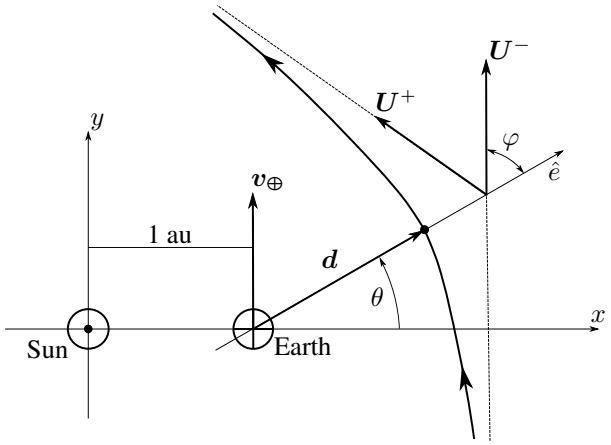

Fig. 1: Kinematics of the close encounter at $t = 0$ (scale exaggerated for clarity). The asymptotic velocity vectors at entry in and exit from the close encounter are designated with $\boldsymbol{U}^-$, $\boldsymbol{U}^+$, respectively. The eccentricity vector is designated with $\boldsymbol{e}$. The asymptotes of the hyperbolic trajectory are represented with dashed lines.

radius" $R_{\rm sw}$. The rationale behind this approach, which we dubbed "Online Trajectory Matching" (OTM), will become apparent in Section 4.1.

We highlight that the focus of the study is to compare different *dynamical formulations*, that is different sets of ODEs representing the physical model in question. It is not our aim to compare different *numerical solvers*, which consist of the algorithms (numerical scheme, local truncation error control, step-size and order control, ...) used to solve such sets of ODEs. In fact, the problem of finding the numerical solver which best fits a dynamical formulation is still open and deserves further work [9]. In all the numerical tests presented here we adopted the same numerical integrator, whose characteristics are described in Section 4.2.

4.1. Online Trajectory Matching (OTM)

Online Trajectory Matching (OTM) is a simple algorithm aimed at increasing the computational efficiency of element methods in interplanetary orbit propagations with close encounters. Such methods perform well for weakly perturbed problems, while close encounters introduce a strong, impulse-like perturbation on a heliocentric scale. OTM decomposes the strongly-perturbed heliocentric problem with a close encounter in three weakly-perturbed phases, with distinct dynamics:

1. Phase H- (heliocentric, pre-encounter): the Sun is the primary body and the planet is the perturbing body; the motion is referred to the Sun.

2. Phase CE (close encounter/planetocentric): the planet is the primary body and the Sun is the perturbing body; the motion is referred to the Earth.

3. Phase H+ (heliocentric, post-encounter): same dynamics as phase H-.

The propagation starts in phase H-, and it is carried out until the geocentric distance R satisfies the switch criterion $R \leqslant R_{\rm sw}$, where $R_{\rm sw}$ is the pre-defined switch radius. At this instant, we pass from phase H- to phase CE and both the state vector and the numerical scheme are re-initialized. The propagation continues in phase CE (planetocentric) until we have $R \geqslant R_{\rm sw}$; the motion is then referred again to the Sun until the final time of the propagation or a potential next encounter.

The algorithm is analogous to the matched-conics method, however in OTM the PCR3BP is preserved along the whole propagation, i.e. no two-body approximation is made. Moreover, the increase of the magnitude of the gravitational perturbation as the particle is approaching the Earth can be contained by considering the appropriate reference system for each phase of the propagation.

The OTM algorithm also allows to use a different formulation for each phase, which can increase the overall propagation efficiency [6].

4.2. Solver

The solver used in all the numerical experiments is the `LSODAR` Fortran subroutine. It is part of the `ODEPACK` library, whose Fortran 77 codes are freely available online[1].

`LSODAR` is a numerical solver with dense output using two multistep and implicit numerical schemes of the predictor-corrector type, namely the Adams-Moulton (AM) and the backward differentiation (BDF) formulas [15]. The latter scheme is used in case that `LSODAR` detects that a problem is becoming stiff [16]; for non-stiff problems and for initializing the integration `LSODAR` uses the AM formulas. Due to stability considerations, the order of the methods is limited to 12 for the AM formulas and 5 for the BDF.

Both the step size and the order of these schemes vary during the integration depending on the instantaneous estimate of the local truncation error. This characteristic is particularly important when propagating without OTM, since it allows the solver to accommodate the sharp increase in perturbations caused by a close encounter.

An appealing characteristic of this solver is its root-finding capability. Let $\boldsymbol{y}(s)$ be the vector solution, function of the independent variable s. At each step, `LSODAR` searches for the roots of a user-assigned set of algebraic equations $\boldsymbol{g}(\boldsymbol{y}, s) = \boldsymbol{0}$ through a bisection method [17]. If a root s^* is found for one of the equations, the integration stops and the output $\boldsymbol{y}^* = \boldsymbol{y}(s^*)$ is returned to the user. As explained in Section 2.1, a root-finding capability is mandatory if output is needed at user-assigned values of physical time. In our case,

[1] `https://computation.llnl.gov/casc/odepack/`

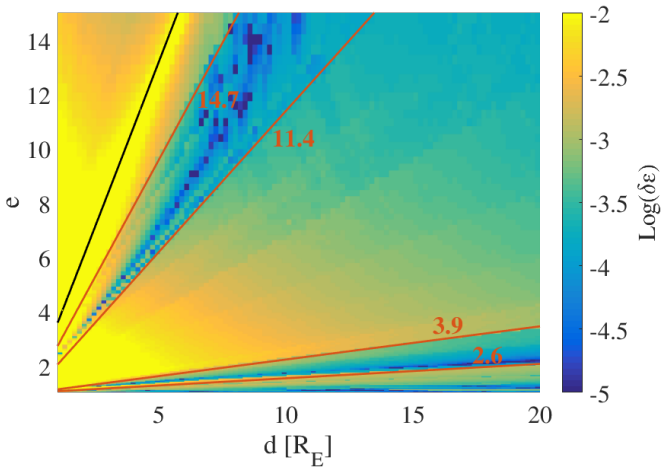

Fig. 2: Relative energy error as a function of the minimum approach distance (d) and the eccentricity of the geocentric hyperbola (e) for the Cowell formulation. We set $\theta = 0°$ (Section 3.1), `tol` = 10^{-6} (Section 6.1). Isolines of the encounter energy are shown in red and are labelled with the corresponding value of the asymptotic velocity U in km/s. The locus of parabolic heliocentric orbits ($\varepsilon^{\mp} = 0$) is indicated by a black line. The distance d is in Earth radii.

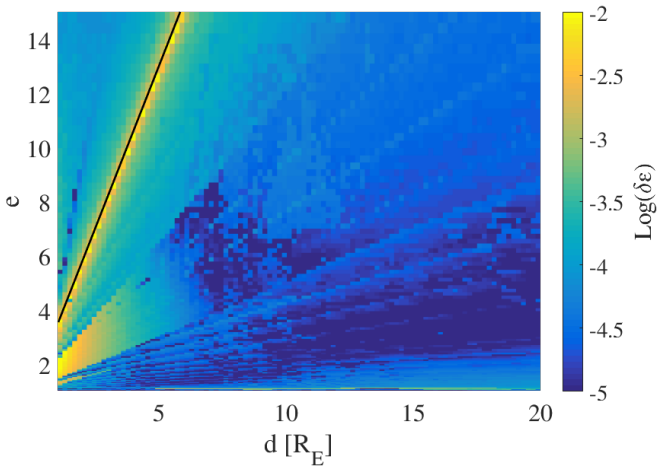

Fig. 3: Relative energy error as a function of (d, e) for the Kustaanheimo-Stiefel formulation. We set $\theta = 0°$, `tol` = 10^{-6}. The locus of parabolic heliocentric orbits ($\varepsilon^{\mp} = 0$) is indicated by a black line. The distance d is in Earth radii.

the root-finder was also used to check the fulfilment of the switch criterion in the OTM algorithm.

5. PERFORMANCE METRICS

The most critical orbital element to be propagated during a close encounter is the heliocentric energy, or equivalently the semi-major axis. This is because errors in semi-major axis will produce errors in the period, thus leading to a secular growth of the positional error. Because of this, we took as an accuracy metric the relative difference between the reference and test heliocentric energies,

$$\delta\varepsilon = \left| \frac{\varepsilon_{\text{test}} - \varepsilon_{\text{ref}}}{\varepsilon_{\text{ref}}} \right|, \tag{7}$$

evaluated at the end of the propagation time span.

We took the number of evaluations of the right-hand side of the equations of motion as a metric of computational effort. This measure is independent from the particular machine used or implementation of the software. It also provides a good estimation of the required computational time when complex physical models are used, as is often the case in numerical propagations.

6. NUMERICAL ANALYSIS

We evaluated the performance of the formulations in Table 1 by propagating a large set of close encounters parametrized in (d, e, θ). In the following sections, we will describe the set-up of the numerical experiments and analyse the results from propagations carried out both with and without using the OTM algorithm. Moreover, we analysed the performance impact of different criteria for switching between the heliocentric and planetocentric phases when the OTM algorithm is used.

6.1. Numerical set-up

For each set of parameters (d, e, θ) we obtained a reference solution covering a time span $\Delta t = 6$ months before and after the encounter. This solution was computed in quadruple precision using the Cowell formulation in heliocentric coordinates, with the relative and absolute tolerances of the solver set to 10^{-23}.

The performance of the aforementioned propagation methodologies was evaluated by running "test" propagations which start six months before the encounter time and are stopped six months after the encounter. Therefore the total duration of the propagations is fixed to 1 year. The choice of the time span Δt is a compromise between two limiting factors. On one hand, an inferior limit to Δt must be set to allow some accumulation of numerical error before the encounter. On the other hand, the time interval Δt cannot be too large, otherwise the final numerical error would be mainly due to the accumulation during the heliocentric phases and not to the close encounter itself, thus defying the purpose of the analysis. Moreover, a large Δt increases the probability of experiencing one or more close encounter after the first, which would unnecessarily complicate our study.

Each "test" propagation was performed in double precision. The relative and absolute tolerances of the solver al-

Table 2: Relative energy error and total number of right-hand-side evaluations averaged over the (d, e) plane for the Cowell (Cow), Kustaanheimo-Stiefel (K-S) and EDromo (EDr) formulations without the Online Trajectory Matching described in Section 4.1.

		Avg. error			Avg. evals		
tol	θ (°)	Cow	K-S	EDr	Cow	K-S	EDr
10^{-6}	0	3.84×10^{-3}	2.01×10^{-4}	2.23×10^{-3}	374	386	979
10^{-6}	90	6.46×10^{-3}	5.38×10^{-4}	4.48×10^{-3}	404	374	870
10^{-12}	0	8.36×10^{-9}	2.82×10^{-9}	7.87×10^{-9}	1330	1436	3281
10^{-12}	90	1.21×10^{-8}	1.47×10^{-8}	2.00×10^{-8}	1507	1345	3129

ways have the same values: $\texttt{rtol} = \texttt{atol} = \texttt{tol} = 10^{-6}$ or $\texttt{tol} = 10^{-12}$.

6.2. Performance analysis in heliocentric propagations

The propagation accuracy of the Cowell and Kustaanheimo-Stiefel formulations can be assessed from Figures 2 and 3, which show the relative error in the final heliocentric energy as a function of (d, e) for $\theta = 0°$. As to interpret the plots, one must remember that each point in the (d, e) plane corresponds to a different set of pre- and post-encounter heliocentric orbital elements. Most importantly, the pre- and post-encounter heliocentric orbital energies are equal under the matched-conics approximation and increase with U, as follows from Equation (5). The black line in both of the figures divides the (d, e) plane in two regions: the one above the line corresponds to hyperbolic heliocentric orbits and the other one to elliptic heliocentric orbits. Points in the right part of the plane, corresponding to shallow close encounters with low perturbing accelerations, have low error values. As expected, when going towards lower values of d the magnitude of the error increases, especially with the Cowell formulation. Moreover, for both Cowell and Kustaanheimo-Stiefel, the encounters that occur closer to the Earth are propagated less accurately when moderate Earth-particle relative velocities are involved. The error growth in this regime is only partially mitigated by the type of propagation method and the solver's adaptive numerical scheme.

For both formulations, the error magnitude exhibits quite steep variations (up to two orders of magnitude) for neighbouring close encounter conditions. This is due to the adaptive scheme employed by the solver; when going from a higher to a lower error region through these "error jumps", LSODAR increases the order of the numerical scheme as to satisfy the internal constraints on the local truncation error. The loci of these jumps closely match the isolines of the encounter energy. As it is evident from Figure 4 this behaviour appears also when using other formulations, thus it seems to be completely related to the type of solver used.

In Figures 2 and 3, the steep increase in the error magnitude around the locus of parabolic heliocentric orbits is an artefact of the particular error metric used, since $\varepsilon^{+}_{\text{ref}} \approx 0$ in that region. The error in the hyperbolic region is greater than the one in the elliptic region for both formulations, however this error increase is more contained for Kustaanheimo-Stiefel. In general, this last formulation achieves lower error values in the whole (d, e) plane, confirming the advantages of integrating regularized equations even when using an adaptive numerical scheme.

It was also interesting to investigate the performance of the EDromo regularized element formulation, without applying any switch of the primary body during the propagation. The formulations were compared by looking at the relative energy error and the total number of evaluations of the right-hand side of the equations of motion. For a given value of θ, we averaged both these quantities over the region $(d, e) = [1, 20]R_{\oplus} \times [1.01, 15]$ of the parameter space. For fairness of comparison, we excluded from the averaging the pairs (d, e) corresponding to hyperbolic heliocentric orbits, since these were not propagated with the EDromo formulation.

Table 2 shows the results for $\texttt{tol} = 10^{-6}, 10^{-12}$ and $\theta = 0°, 90°$. The Kustaanheimo-Stiefel formulation exhibits the best efficiency for a tolerance of 10^{-6}, and it reduces the error by one order of magnitude with respect to the Cowell formulation. This advantage is somewhat mitigated for the tighter tolerance 10^{-12}. Integrating the EDromo equations allows to reach accuracies which are comparable or lower than Cowell's, however this is to the expense of the number of evaluations. The increase in the number of right-hand-side evaluations signals more effort spent by the numerical scheme to follow the perturbations with the requested accuracy; the adoption of the OTM algorithm to reduce the perturbing acceleration magnitude is then justified.

6.3. Performance analysis with OTM

The Online Trajectory Matching was applied in combination with the regularized element methods in Table 1: *EDromo* was used to propagate the heliocentric phases H-/H+, while *HDromo* was used for the hyperbolic phase CE. This is possi-

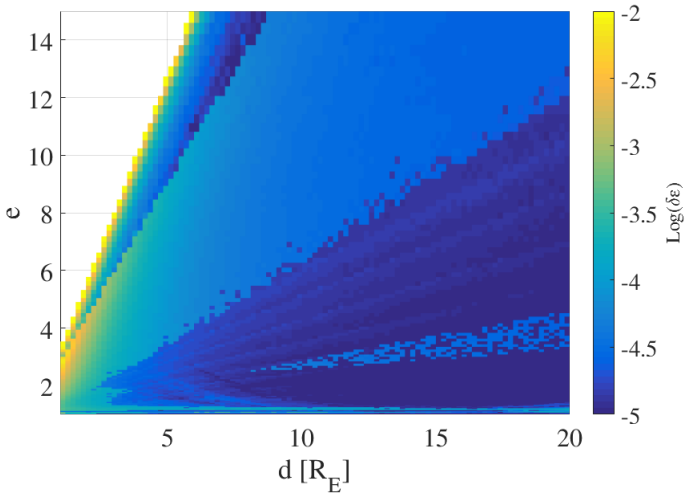

Fig. 4: Relative energy error as a function of (d, e) for the regularized element methods EDromo, HDromo with the Online Trajectory Matching (Section 4.1). We set $\theta = 0^\circ$, $\texttt{tol} = 10^{-6}$, $R_{\rm sw} = 5.53\, R_{\rm SoI}$. Hyperbolic heliocentric trajectories were not propagated. The distance d is in Earth radii.

ble since the three phases are completely independent from each other; the integration is restarted at the beginning of phases CA/H+ from the final conditions reached at the end of the previous phase.

Figure 4 displays the magnitude of the relative energy error at the end of the propagations using OTM and regularized element methods for the same θ and $\texttt{tol}$ of Figure 2. The switch radius was set at $R_{\rm sw} = 5.53\ R_{\rm SoI}$, where $R_{\rm SoI} = a_\oplus \left(\mu_\oplus/\mu_\odot\right)^{2/5} \approx 925000$ km is the radius of the Earth's sphere of influence. As it will be shown in the next Section, this choice allows to obtain a lower average error with respect to the case $R_{\rm sw} = 1\, R_{\rm SoI}$.

By comparing the two figures we notice that this propagation strategy allows to reduce the final relative energy error by about two orders of magnitude with respect to Cowell. The performance of the element methods when combined with the OTM strategy is substantially improved with respect to the purely heliocentric propagation carried out with EDromo (Table 2). This is due to the fact that by employing OTM we are effectively decreasing the perturbation magnitude during each phase of the propagation.

The error behaves in a way similar to the Cowell and Kustaanheimo-Stiefel formulations. Bigger errors are still reached for encounters that occur closer to the Earth. Among them the most difficult to propagate are those characterized by higher energies, i.e. faster encounters. However, the performance is more satisfactory in this region.

The white area in the top left of the plot is relative to hyperbolic heliocentric orbits. Since the method used in phases H-/H+ works for negative values of the total energy, it was not possible to propagate this set of initial conditions. This issue can be easily solved by using an appropriate method depending on the sign of the total energy. Nevertheless, we chose to consider only the set of points (d, e) corresponding to elliptic orbits since it contains the most interesting cases from the standpoint of Space Situational Awareness, with orbit characteristics similar to those of NEAs.

6.4. Impact of the switch criterion in OTM

We conclude our analysis by looking at a subtle aspect of Online Trajectory Matching which deserves some attention. Up to now, we have implied that the switch between the different phases takes place at a pre-defined planetocentric "switch radius" $R_{\rm sw}$, but we have not mentioned any criterion leading to its choice. Several criteria for distinguishing between the regions of gravitational influence attaining to different celestial bodies exist in the literature; the most widely known are the Hill sphere and the Laplace sphere of influence. However, we remind that our study is aimed at minimizing the final propagation error at the end of the numerical integrations; finding a criterion which guarantees such objective is not trivial. Ideally, it should allow to decrease the magnitude of the perturbing accelerations, thus reducing the global numerical error. This task is complicated by the particularities connected with using regularized formulations and element methods.

As a first step in this direction, we carried out the propagations in the region $(d, e) = [1, 20] R_\oplus \times [1.01, 15]$ for different values of the switch radius. The relative energy errors and the corresponding number of right-hand-side evaluations were averaged over all the considered points (d, e). The resulting values are shown in Figures 5 and 6 for several switch radii. These figures were obtained by setting $\texttt{tol} = 10^{-6}$ and $\theta = 0^\circ, 90^\circ$ respectively. The switch radius has a relevant impact on the final propagation error, as in some cases different values of $R_{\rm sw}$ give origin to variations of up to one order of magnitude in $\delta\varepsilon$ (Figure 6a). Moreover, the switch radius which minimizes $\delta\varepsilon$ is not always located at $1 R_{\rm SoI}$, and it depends on θ. In fact, for $\theta = 0^\circ$ the average error can be reduced by a factor of 3 by switching primary bodies at $7\, R_{\rm SoI}$ instead of at $1\, R_{\rm SoI}$. A switch criterion based on purely dynamical considerations, such as the Laplace sphere of influence, does *not* guarantee the best numerical performances in our approach.

Another requirement driving the choice of the switch radius regards the reliability of the integration. Both the formulations chosen in the propagations with the OTM algorithm are particularized to either negative or positive total energy, and lose meaning if this sign changes during the propagation. In this paper, all the close encounters occur on hyperbolic geocentric trajectories. Besides, heliocentric arcs are elliptical. However, we noticed that in some cases, especially when the close encounter is extremely slow, the total energy computed along the geocentric trajectory changes sign (i.e. becomes negative) when the propagated body is far from the

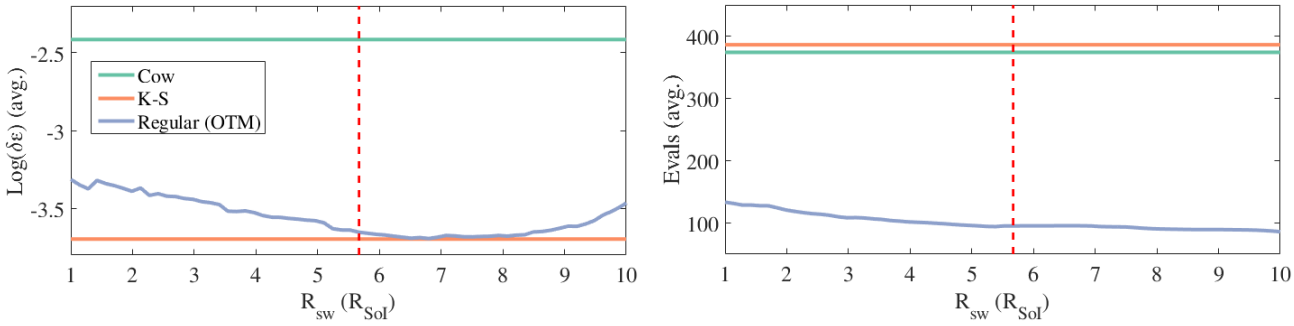

(a) Relative energy error

(b) Right-hand-side evaluations

Fig. 5: Average relative energy error and number of right-hand-side evaluations as a function of the switch radius $R_{\rm sw}$. We set $\theta = 0^\circ$, $\texttt{tol} = 10^{-6}$. The blue curve refers to the regularized element methods EDromo, HDromo with OTM. The green and orange lines refer to the Cowell and Kustaanheimo-Stiefel formulations in the heliocentric system. These lines represent the values reported in Table 2. The dashed red line corresponds to the smallest switch radius for which at least one pair (d, e) leads to a change of sign of the total energy in the geocentric phase.

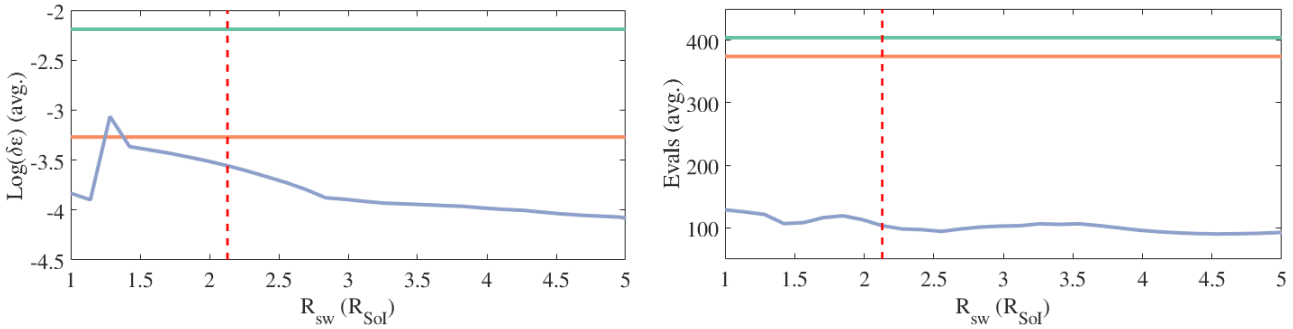

(a) Relative energy error

(b) Right-hand-side evaluations

Fig. 6: Same as in Figure 5, for $\theta = 90^\circ$, $\texttt{tol} = 10^{-6}$.

Earth. In such cases the propagation stops, since the formulation which is being used in this phase works for strictly positive values of the total energy. This happens more frequently the higher the switch radius, or equivalently the longer the CE phase. This is easily understood from the dynamical standpoint, since the motion for distances sufficiently far from the Earth is actually dominated by the Sun and thus the geocentric energy exhibits very strong variations. In Figures 5 and 6 we have marked the first value of $R_{\rm sw}$ for which there is at least one pair (d, e) which leads to this phenomenon. The points (d, e) producing this change of sign of the total energy were not counted in the averaging computation of the error and of the vector field evaluations.

The dependence of the computational cost on the switch radius is very weak. In any case, the approach using regularized element methods with OTM exhibits a number of right-hand-side evaluations which is four times smaller than that of the Cowell and Kustaanheimo-Stiefel formulations, while maintaining an average error which is comparable to that of the K-S.

7. CONCLUSIONS

In this work, we assessed the computational efficiency of novel propagation techniques of interplanetary trajectories with close encounters.

The behaviour of the regularized element methods EDromo [7] and HDromo [8] was investigated by performing large-scale numerical simulations in the planar CR3BP. We included in our analysis also the Cowell formulation (i.e. the unregularized equations of motion for rectangular Cartesian coordinates) and the Kustaanheimo-Stiefel formulation. The numerical integrator employs variable step-size and order multistep numerical schemes.

If the propagation is carried out in a heliocentric reference system the Kustaanheimo-Stiefel formulation gives the best efficiency, achieving a value of the final propagation error which is up to one order of magnitude lower than the Cowell formulation with the same computational cost.

A novel algorithm, *Online Trajectory Matching*, was devised to decompose the strongly-perturbed heliocentric close encounter problem in three weakly-perturbed phases, asso-

ciated with three propagation phases: pre-encounter (heliocentric), encounter (planetocentric) and post-encounter (heliocentric). This algorithm greatly increases the efficiency of the propagation when using regularized element methods, given that the planetocentric distance at which the primary body is switched is chosen carefully.

With the proposed approach, it is possible to achieve the same accuracy as the Kustaanheimo-Stiefel formulation but with a computational cost four times smaller.

8. ACKNOWLEDGEMENTS

This work is funded by the European Commission's Framework Programme 7, through the Stardust Marie Curie Initial Training Network, FP7-PEOPLE-2012-ITN, Grant Agreement 317185. D. Amato would like to thank G.B. Valsecchi for the stimulating suggestions received during the author's visiting period at the Institute of Applied Physics of the Italian National Research Council.

9. REFERENCES

[1] E.J. Öpik, *Interplanetary Encounters*, Elsevier Scientific Publishing, Amsterdam, NL, 1976.

[2] G.B. Valsecchi, A. Milani, G.F. Gronchi, and S.R. Chesley, "Resonant returns to close approaches: Analytical theory," *A&A*, vol. 408, pp. 1179–1196, 2003.

[3] G.B. Valsecchi, "Geometric conditions for quasi-collisions in Öpik's theory," *Lect. Notes Phys.*, vol. 682, pp. 145–158, 2006.

[4] F. Debatin, A. Tilgner, and F. Hechler, "Fast numerical propagation of interplanetary orbits," in *ESA Proceedings of the Second International Symposium on Spacecraft Flight Dynamics*. European Space Agency, 1986, pp. 329–333.

[5] E.L. Stiefel and G. Scheifele, *Linear and Regular Celestial Mechanics*, Springer-Verlag, Berlin, Germany, 1971.

[6] D. Amato, C. Bombardelli, and G. Baù, "Mitigation of propagation error in interplanetary trajectories," *Adv. Astronaut. Sci.*, vol. 155, pp. 1003–1020, 2015.

[7] G. Baù, C. Bombardelli, J. Peláez, and E. Lorenzini, "Non-singular orbital elements for special perturbations in the two-body problem," *Mon. Not. R. Astron. Soc.*, vol. 454, pp. 2890–2908, 2015.

[8] G. Baù, D. Amato, C. Bombardelli, and A. Milani, "New orbital elements for accurate orbit propagation in the solar system," in *Proceedings of the 6th International Conference on Astrodynamics Tools and Techniques (ICATT)*. European Space Agency, 2016.

[9] H. Urrutxua Cereijo, *High Fidelity Models for Near-Earth Object Dynamics*, Ph.D. thesis, Technical University of Madrid, School of Aeronautical Engineering, Madrid, Spain, 2015.

[10] V.R. Bond and M.C. Allman, *Modern Astrodynamics: Fundamentals and Perturbation Methods*, Princeton University Press, Princeton, NJ, USA, 1996.

[11] J. Geul, E. Mooij, and R. Noomen, "Regularised methods for high-efficiency propagation," in *Proceedings of the 2015 AAS/AIAA Specialist Conference*, Vail, CO, USA, 2015, American Astronautical Society.

[12] G.R. Hintz, "Survey of orbit element sets," *J. Guid. Control. Dynam.*, vol. 31, no. 3, pp. 785–790, 2008.

[13] J. Peláez, J.M. Hedo, and P. Rodríguez de Andrés, "A special perturbation method in orbital dynamics," *Celest. Mech. Dyn. Astr.*, vol. 97, no. 2, pp. 131–150, 2007.

[14] S. Kemble, *Interplanetary Mission Analysis and Design*, Praxis Publishing, Chichester, UK, 2006.

[15] K. Radhakrishnan and A.C. Hindmarsh, "Description and use of LSODE, the Livermore solver for ordinary differential equations," Tech. Rep. UCRL-ID-113855, Lawrence Livermore National Laboratory, 1993.

[16] L. Petzold, "Automatic selection of methods for solving stiff and nonstiff systems of ordinary differential equations," *SIAM J. Sci. Stat. Comp.*, vol. 4, no. 1, pp. 136–148, 1983.

[17] K.L. Hiebert and L.F. Shampine, "Implicitly defined output points for solutions of ODEs," Tech. Rep. SAND80-0180, Sandia Laboratories, 1980.